BNL--45045

DE92 007613

ELECTROCHEMICALLY INDUCED RECONSTRUCTION OF THE Au(001) SURFACE: AN X-RAY SCATTERING STUDY

B.M. Ocko and Jia Wang
Physics Department
Brookhaven National Laboratory
Upton, New York 11973

ABSTRACT

In-situ x-ray specular reflectivity and glancing incident angle x-ray diffraction measurements have been performed in the Au(001) surface in two solutions under potential control in an electrochemical cell. In both the 0.01 M $HClO_4$ and 0.01 M KBr solutions a "(5×20)" reconstruction is formed at sufficient negative potentials. The reconstruction is similar to that obtained for the clean surface in vacuum.

The utilization of surface x-ray scattering techniques (SXS), scanning tunneling microscopy (STM), and atomic force microscopy (AFM) techniques during the past decade has greatly enhanced our understanding of surfaces in vacuum. Currently, these same techniques are rapidly being utilized to study electrode surfaces on an atomic scale with an increasing level of sophistication [1-6]. Here we report the principle results of a SXS study of the Au(001) electrode surface in an acid solution (0.01 M $HClO_4$) and in a salt solution (0.01 M KBr). In a SXS measurement the diffracted intensity couples directly to the periodicity of the top several layers of metal atoms. This facilitates a direct in situ measurement of the phase behavior versus the applied potential with a high degree of accuracy.

In vacuum, the Au(001) surface exhibits a hexagonal reconstruction where there are nearly six surface atoms for every five bulk atoms along the [110] direction [7-10]. The reconstruction is often referred to as "5×20" although the actual top layer is more accurately described as incommensurate [9]. The in-plane surface diffraction (see Figure 1a) is described by a hexagonal pattern centered around the origin with a wavevector $\sqrt{2}\Delta_1 a^*(\Delta_1 = \Delta_2)$, where the incommensurability $\delta = \Delta_1 - 1 = 0.206 \pm 0.001$ [8,11], $a^* = 2\pi/a$, and where $a = 4.081$ Å is the size of the face centered cubic unit cell for Au. The orientation of the reconstructed layer is rotated by $\pm 0.8°$ from the [110] axis, with a surface corrugation amplitude of $\lesssim 0.50$ Å peak-peak [9,11,12], has 25% excess mass relative to the underlying bulk layers [13,14] and a 20% interlayer expansion [14]. The excess mass and the expansion nearly conserve the bulk packing density.

The present study has been motivated by extensive electrochemical studies of the Au(001) surface [15,16]. From measurements of the potential of zero charge (PZC) [15,16] which is related to the work function, optical reflectivity(OR) [16]

and second harmonic generation [17] it has been inferred that a potential change can induce a surface structural transition. Ex-situ low energy electron diffraction measurements [18], after emersion from an electrochemical cell, suggest that the structural transition inferred from the PZC and OR measurements corresponds to the lifting of the hexagonal reconstruction. More recently, STM studies of the Au(001) surface in $HClO_4$ solutions [6] have directly imaged the hexagonal reconstruction with atomic resolution under potential control.

In the present paper, we report the results of an x-ray scattering study from the Au(001) electrode in $HClO_4$ and KBr electrolytes. The structure of the gold surface has been determined at fixed potentials. In addition, the potential dependence of the scattering has also been measured. The x-ray measurements in $HClO_4$ have been previously reported [4].

Two types of x-ray scattering measurement were carried out. In-plane surface x-ray diffraction measurements, with the x-rays incident at a very shallow ($\sim 2°$) angle to the surface, has been used to determine the crystallographic structure of 2-D surface overlayers. X-ray specular reflectivity measurements have been used to determine the electron density profile in the direction normal to the surface. The reflectivity data provides information on the density, roughness and interlayer spacing of atomic layers parallel to the crystal surface. These two independent and complementary measurements can be used together to give a detailed picture of surface structure.

Fig. 1(a) shows the electrochemical cell. A 6μm polypropylene window covers and seals the cell with a thin capillary film ($< 20\mu$m) between the metal surface and the polypropylene film. A detailed description of the apparatus is presented elsewhere [4,19]. Loss of signal due to absorption of the x-rays by the solution and the polymer film is small since the absorption length of x-rays in these materials is several millimeters for x-rays of 10 keV.

The in-plane diffraction pattern for the Au(001) surface, is shown in Fig. 1(b). Fig. 2(a) shows a scan across the hexagonal diffraction point $(\Delta_1, \Delta_1, 0)$ for 0.01 M $HClO_4$. This rocking curve exhibits two distinct peaks for the approximate hexagonal reconstruction at low potentials (open circles). The rotation of the hexagonal reconstructed layer with respect to the [110] direction agrees with the 0.8° rotation angle obtained under vacuum conditions [9,10]. Above 0.5 V, the surface scattering vanishes as shown in Fig. 2(a) (closed circles). At these potentials, the reconstructed layer has lifted and only surface reflections corresponding to the bulk (square symmetry, see Fig. (1b)) are observable. The presence of the reconstructed phase has been determined by integrating the rocking curves at the hexagonal positions shown in Fig. 2(a). Fig. 2(b) shows this integrated intensity as a function of potential across the transition region between 0 and 0.6 V at an effective scan rate of 0.004 mV/sec.. The integrated intensity starts to decrease at about 0.20 V, falls to half at 0.35 V, and nearly vanishes by 0.50 V. The transition occurs at somewhat higher potentials when the scan rate is increased.

At negative potentials, the in-plane diffraction features a near hexagonal pattern with $\Delta_1 = 1.205 \pm 0.002$ and $\Delta_2 = 1.200 \pm 0.005$ where Δ_1 and Δ_2 are the magnitude

of the hexagonal wavevector along the [110] and rotated directions as shown in Fig. 3. The incommensurability, is in near perfect agreement with vacuum studies of the Au(001) surface [9-10]. There is a small change in Δ_1 and virtually no change in Δ_2 with potential. This is in contrast to the Au(111) surface where the stripe separation changes continuously from p=23 at the most negative potentials to p=30 before the reconstruction lifts [19]. We do not observe a corresponding continuous transition at the Au(001) surfaces.

The surface normal distribution of the electron density profile can be directly related to the specular reflectivity profile. In a specular reflectivity measurement the scattered intensity, along the surface normal wavevector, is measured on an absolute scale [19]. Fig. 3(a) shows the specular reflectivity for the reconstructed (-0.4 V, open circles) and lifted (+1.0 V, closed circles) surface structures in 0.01 M $HClO_4$. There are distinct differences between these two curves which are most apparent at $L = 1$ where the reflectivity differs by a factor of 5. The specular reflectivity $R(Q_z)$ where $Q_z = 2\pi L/a$ can be modeled as a sum over atomic layers

$$R(Q_z) \propto \left| \sum_{m=0}^{\infty} < \rho_m e^{-Q_z^2 \sigma_m^2/2} e^{iQ_z(a/2)(m-\epsilon)} > \right|^2$$

where the proportionality factor can be calculated from fundamental constants. Each term in the sum corresponds to an atomic layer m where ρ_m is the electron density relative to a bulk (001) layer, ϵ_m is the increase in atomic interlayer spacing relative to a bulk (001) layer and σ_m is the root-mean-square (r.m.s.) atomic displacement.

For a perfectly terminated crystal (square symmetry), the calculated specular reflectivity is shown in Fig. 4(a) (broken line). It does not agree with data from either the reconstructed or the lifted surfaces. At -0.4 V (reconstructed surface), an excellent fit to the data (Fig. 4(a), solid line) is obtained for a top layer density of 1.21 with a 20% outward expansion of the top gold layer, relative to the bulk gold-gold layer spacing of 2.04 Å. The excess density and expansion of the top layer are in close agreement with the close-packed hexagonal layer found in vacuum [9,11]. At +1.0 V, the best fit is obtained with a top layer density of 0.22 and no expansion of the interlayer spacing for the top layer of gold. Constraining the top layer density to unity causes a dramatic increase in the error of the fit. At the Au(111) electrode surface, adsorbed electrolyte species modify the observed reflectivity [19]. This effect has not been included in the analysis of the Au(001)/electrolyte interface.

The transition between the reconstructed and the lifted surfaces can be repeated on cycling the potential. Fig. 4(b) shows the voltage dependence of the reflected intensity at $(0, 0, 2.3)$ for two different potential scan rates in the $HClO_4$ solution. The lower scan rate shows a smaller hysteresis for the two scan directions. We note that in the forward sweep direction, the intensity at the wavevector $(0, 0, 2.3)$ increases when the reconstructed layer lifts. This is because the asymmetry in the reflectivity, in the wings of the (002) Bragg peak (see Fig. 4(a)), vanish when the surface transforms from the reconstructed to a (1x1) surface layer. The change

in intensity shown in Fig. 4(b) is primarily due to changes in the density of the gold layers and not due to anion adsorption. The latter has been observed at the Au(111) electrode surface in salt solutions [19].

We have also carried out x-ray diffraction studies of the Au(001) surface in contact with 0.01 M KBr. In salt solutions, the double layer region extends to -0.8 V versus an $Ag/AgC\ell$ reference whereas in 0.01 M $HClO_4$, hydrogen evolution starts at -0.4 V. The in-plane x-ray diffraction pattern is identical to that observed in the $HClO_4$ solution. In Fig. 5 we show the potential dependence of the scattering at three wavevectors; $(1.205, 1.205, 0.3)$, $(1, 1, 0.3)$, and $(0, 0, 2.3)$ at a scan rate of 2 mV/sec. in the 0.01 M KBr electrolyte. The first two wavevectors are in the grazing incident geometry and are sensitive to the in-plane atomic structure. The wavevector $(0, 0, 2.3)$ corresponds to a specular position which is sensitive to the electron density distribution along the surface normal direction. In all three panels of Fig. 5 the diffuse background has been subtracted and the maximum intensity has been normalized to unity.

The scattered intensity at a wavevector $(1.205, 1.205, 0.3)$, rotated by $0.8°$, is sensitive to the order of the hexagonal reconstruction. Above 0.0 V the scattered intensity, after background subtraction, is zero as shown in Fig. 5(a). This is because there is no longer a reconstructed surface layer above this potential. In the negative potential sweep, the reconstruction does not start to form until -0.45 V. Concurrent with the formation of the reconstruction there is a decrease in the scattered intensity at a wavevector $(1, 1, 0.3)$ as shown in Fig. 5(b). This reciprocal space position corresponds to the in-plane periodicity of the underlying gold layers. In the positive direction, the scattered intensity exhibits a dip before the reconstruction is lifted. This reflects a loss of surface order during the lifting process. Similar behavior has been observed at the Au(111) electrode surface in contact with salt solutions [19].

During the reconstruction lifting process, the reflectivity at $(0, 0, 2.3)$ increases, as shown in Fig. 5(c), since the top layer relaxes inward. This occurs at the same potential where the reconstruction is lifted (see Fig. 5(a)). At the most positive potentials, where bromide ions are adsorbed at the surface, the reflectivity is lowered relative to a (1x1) Au surface with no adsorbed bromide ions. This is because the bromide ions interfere destructively with the scattering from the gold layers at $(0, 0, 2.3)$. As the potential is scanned negatively, the reflectivity increases at a potential starting at about -0.1 V. At -0.45 V there is a sharp drop in the reflectivity because the top layer expands outward when the surface reconstructs. Before this drop, the reflectivity continues to increase due to the desorption of bromide ions. In contrast, a plateau (before the drop at -0.45 V) in the reflectivity would have indicated a completion of the bromide desorption process. These findings indicate that bromide ions are still adsorbed at the surface when the reconstruction forms.

The reconstruction lifting/formation transition is much sharper in the KBr solution than in the $HClO_4$ solution (see Fig. 5(c) and Fig. 4(b)). In addition, the potential difference between the reconstruction lifting and formation transitions (i.e. hysteresis) is 0.4 V whereas the corresponding difference in the acid solution is nearly a full volt. In part, we can attribute these differences to kinetic effects

since the surface mobility of gold atoms is enhanced by the adsorption of bromide. Furthermore, the surface charge as a function of applied potential changes faster in the bromide solution than in $HClO_4$ solution. This potential difference is about 0.20 V and 0.10 V for the Au(111) and Au(110) surfaces, respectively, in KBr electrolytes. For Au(001) there is a shift in the PZC (0.12-0.22 V) between the (1x1) and the reconstructed phases on account of the change in symmetry between these two phases [15,16]. This shift explains, in part, why there is the greatest potential hysteresis for the Au(001) surface relative to the (111) and (110) surfaces.

These measurements of the potential induced reconstruction of the Au(001) electrode in contact with $HClO_4$ and KBr solutions demonstrate that important structural information on electrode surfaces can be obtained from in situ surface x-ray scattering experiments. The hexagonal structure of the Au(001) reconstructed electrode in both the acid and salt solution appears nearly identical to room temperature vacuum results. The phase behavior depends very much on the solution species.

This work is supported by the Division of Materials Research, U.S. Department of Energy, under Contract No. DE-AC02-76CH00016.

REFERENCES

1. M.F. Toney and O.R. Melroy, in "In-Situ Studies of Electrochemical Interfaces," H.D. Abruña, Editor, VCH Verlag Chemical, Berlin (1991).
2. J. Wiechers, T. Twomey, D.M. Kolb, and B.J. Behm, *J. Electroanal Chem.*, **248**, 451 (1988).
3. S.L. Yau, X. Gao, S.C. Chang, B.C. Schardt, and M. Weaver, *J. Am. Chem. Soc.*, **113**, 6049 (1991).
4. B.M. Ocko, J. Wang, A. Davenport, and H. Isaacs, *Phys. Rev. Lett.*, **65**, 1466 (1990).
5. S. Manne, P.K. Hansma, J. Massie, V.B. Elings, and A.A. Gewirth, *Science*, **25**, 183 (1991).
6. X. Gao, A. Hamelin, M.J. Weaver, *Phys. Rev. Lett.*, **67**, 618, (1991).
7. P.W. Palmberg and T.N. Rhodin, *Phys. Rev.*, **161**, 586 (1967).
8. G.E. Rhead, *J. Phys. F*, **3**, L53 (1973).
9. S.G.J. Mochrie, D.M. Zehner, D. Gibbs, and B.M. Ocko, *Phys. Rev. Lett.*, **64**, 2925 (1990).
10. D. Gibbs, B.M. Ocko, D.M. Zehner, and S.G.J. Mochrie, *Phys. Rev. B*, **42**, 7330 (1990).
11. B.M. Ocko, D. Gibbs, K.G. Huang, D.M. Zehner, and S.G.J. Mochrie, *Phys. Rev. B*, **44**, 6429 (1991).
12. K.H. Rieder, T. Engel, R.H. Swendsen, and M. Manninen, *Surf. Sci.*, **127**, 223 (1983).

13. D.M. Zehner, B.R. Appleton, T.S. Noggle, J.W. Miller, J.H. Barret, L.H. Jenkins, and O.E. Schow, III, *J. Vac. Sci. Technol.*, **12**, 454 (1975).
14. D. Gibbs, B.M. Ocko, D.M. Zehner, and S.G.J. Mochrie, *Phys Rev. B*, **38**, 7303 (1988).
15. A. Hamelin, *J. Electroanal. Chem.*, 142, 299 (1982); A. Hamelin, *J. Electroanal. Chem.*, **255**, 281 (1988).
16. D.M. Kolb and J. Schneider, *Surf. Sci.*, **162**, 764 (1985).
17. A. Friedrich, B. Pettinger, D.M. Kolb, G. Lupke, R. Steinhoff, and G. Marowsky, *Chem. Phys. Lett.*, **163**, 123 (1989).
18. M.S. Zei, G. Lehmpfuhl, and D.M. Kolb, *Surf. Sci.*, **221**, 23 (1989).
19. J. Wang, B.M. Ocko, A.J. Davenport, and H.S. Isaacs, *Submitted to Phys. Rev. B.*, (1991).

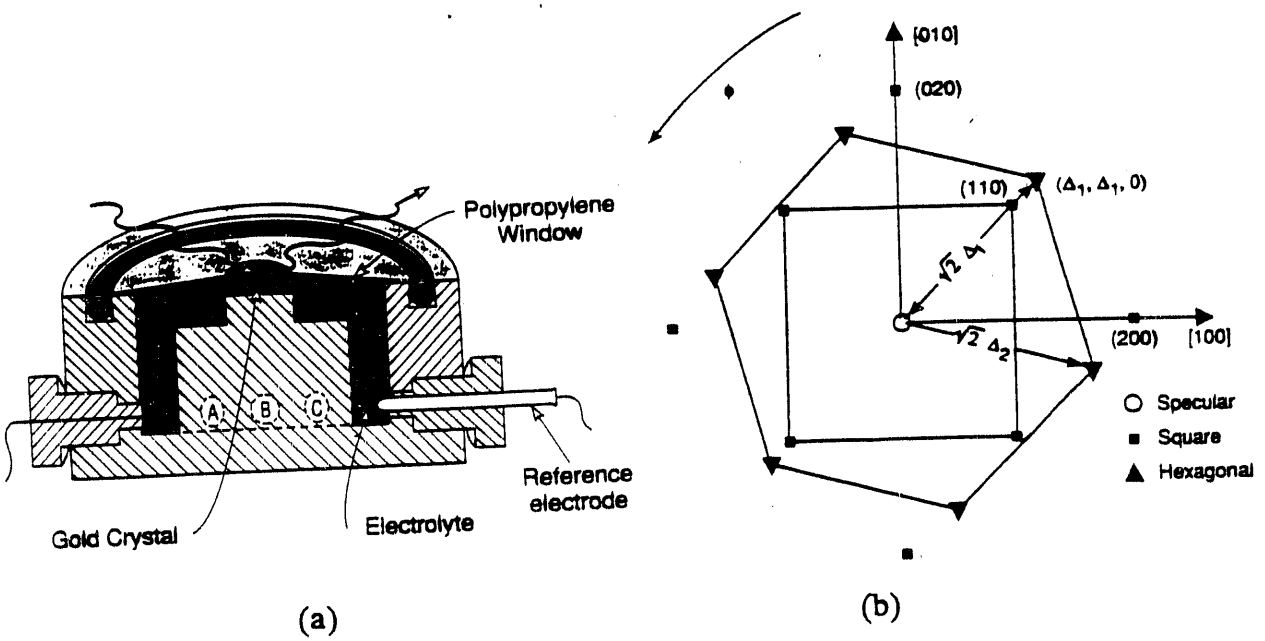

Fig. 1 (a) Electrochemical x-ray scattering Kel-F cell.
(b) In-plane diffraction pattern for the Au(001) surface. The squares show the pattern from the bulk which has square symmetry while the triangles show the pattern from the hexagonal reconstruction which forms at low applied potentials. Each point represents a rod of scattering normal to the surface.

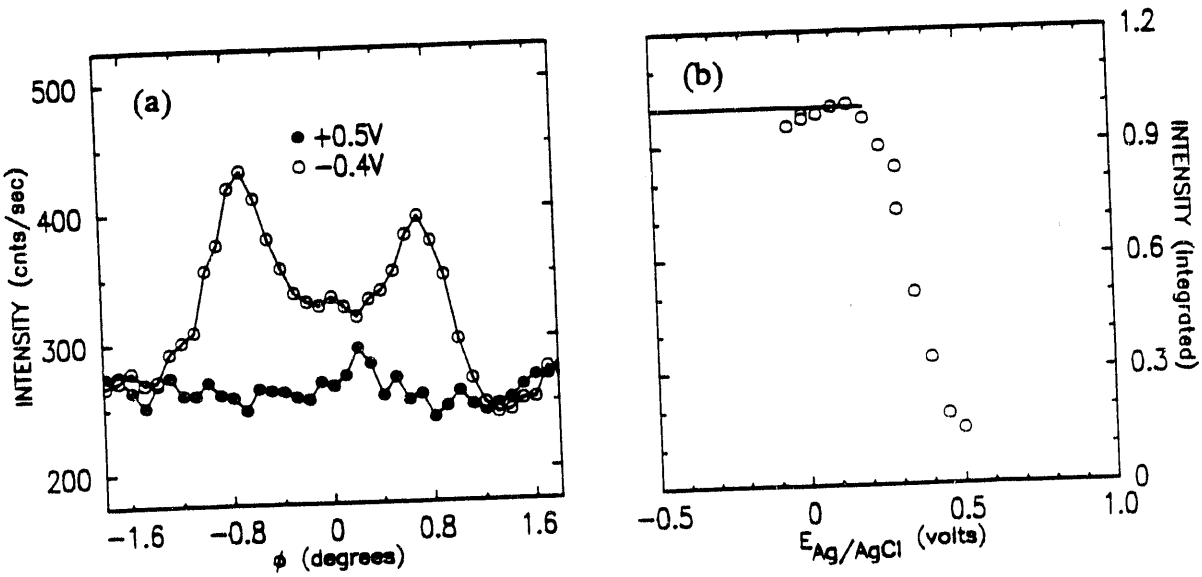

Fig. 2 (a) Glancing incident angle x-ray diffraction rocking curves for -0.4 V and 0.5 V in 0.01 M $HClO_4$ at the primary hexagonal wavevector (1.205, 1.205, 0.3). (b) Potential dependence of the integrated intensity (background subtracted) of the rocking curves shown in (a) upon increasing the potential.

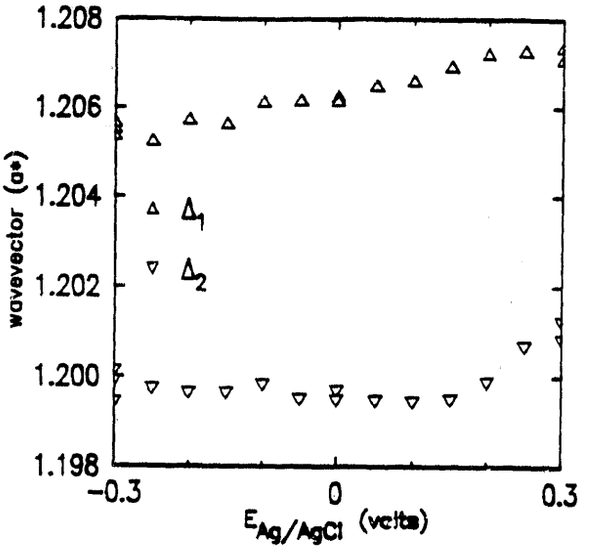

Fig. 3 Potential dependence of the wavevector magnitudes Δ_1 and Δ_2 in 0.01 M $HClO_4$.

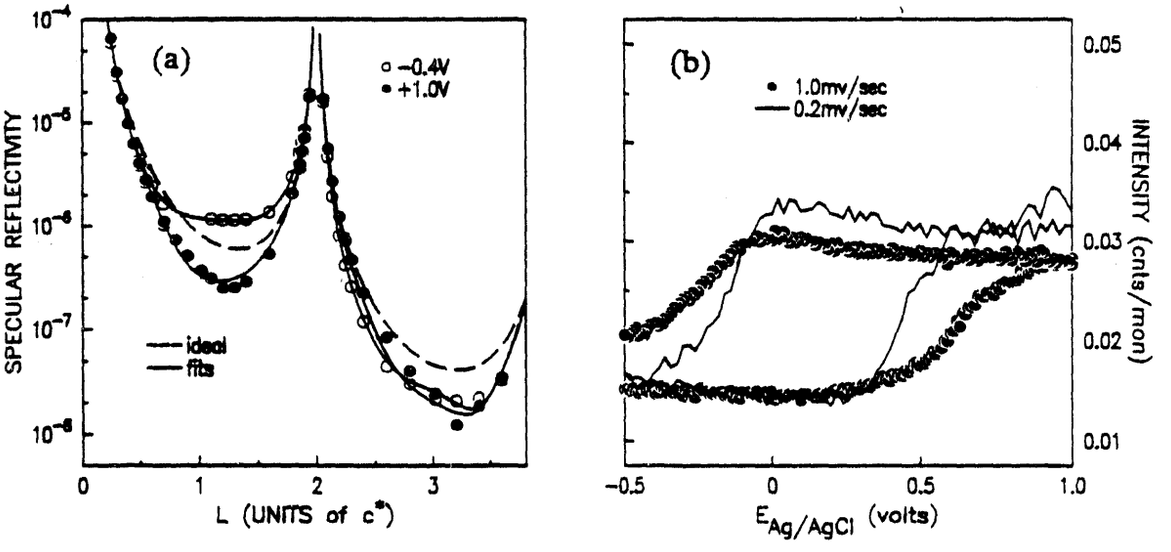

Fig. 4 X-ray reflectivity in from the Au(001) electrode in 0.01 M $HClO_4$.
(a) Absolute reflectivity data for the $(0, 0, L)$ rod at −0.4V (open circles) and 1.0V (closed circles) where $L = aQ_z/2\pi$.
(b) Potential dependence of the specular reflectivity at $(0, 0, 2.3)$ at different potential scanning rates.

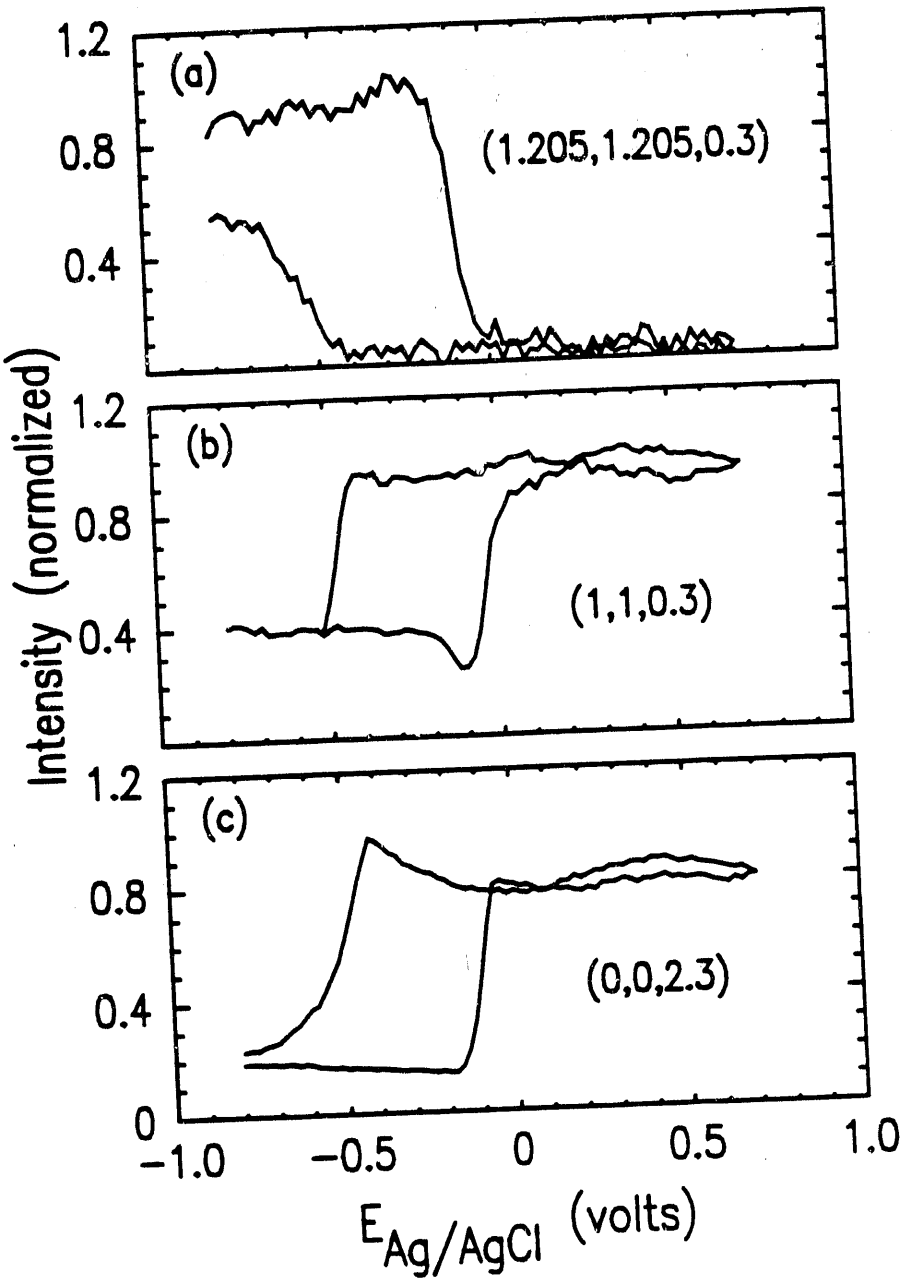

Fig. 5 Potential dependence of the scattered x-rays at the Au(001) surface in contact with 0.01 M KBr at (a) $(1.205, 1.205, 0.3)$ (b) $(1, 1, 0.3)$ and (c) $(0, 0, 2.3)$.

END

DATE FILMED

3/18/92